



THE UNIVERSITY *of* EDINBURGH

Edinburgh Research Explorer

Breaking through permeability–selectivity trade-off of thin-film composite membranes assisted with crown ethers

Citation for published version:

Shen, L, Yi, M, Japip, S, Han, C, Tian, L, Lau, CH & Wang, Y 2021, 'Breaking through permeability–selectivity trade-off of thin-film composite membranes assisted with crown ethers', *AIChE Journal*, vol. 67, no. 6, e17173. <https://doi.org/10.1002/aic.17173>

Digital Object Identifier (DOI):

[10.1002/aic.17173](https://doi.org/10.1002/aic.17173)

Link:

[Link to publication record in Edinburgh Research Explorer](#)

Document Version:

Peer reviewed version

Published In:

AIChE Journal

General rights

Copyright for the publications made accessible via the Edinburgh Research Explorer is retained by the author(s) and / or other copyright owners and it is a condition of accessing these publications that users recognise and abide by the legal requirements associated with these rights.

Take down policy

The University of Edinburgh has made every reasonable effort to ensure that Edinburgh Research Explorer content complies with UK legislation. If you believe that the public display of this file breaches copyright please contact openaccess@ed.ac.uk providing details, and we will remove access to the work immediately and investigate your claim.



23 **Abstract**

24

25 In this study, we deployed a modified interfacial polymerization process to
26 incorporate multifunctional crown ethers (CEs) into thin-film composite (TFC)
27 polyamide membranes. These CE additives acted as both the phase-transfer catalyst
28 and co-solvent to facilitate the diffusion of amine monomers into the organic phase
29 and also enhanced the free volume content of the selective layer, facilitating water
30 transport and inhibiting the diffusion of draw solutes. Various characterization
31 techniques were employed to elucidate the modification mechanism as a function of
32 CE chemical and physical properties on the microstructure of resultant TFC
33 membranes and consequently separation performances. Compared to TFC membranes
34 produced from traditional interfacial polymerization method, CE-modified
35 membranes exhibited a 146% water flux enhancement and 59% lower reverse salt
36 fluxes with a suitable draw solution. CE-modified membranes also exhibited
37 improved antifouling performance with a lower flux drop (34% decline) and a higher
38 flux recovery ratio (38% improvement).

39

40 **Keywords:** Thin-Film Composite Membrane; Polyamide; Crown Ether; Interfacial
41 Polymerization; Permeability-Selectivity Trade-off

42

43 1. INTRODUCTION

44

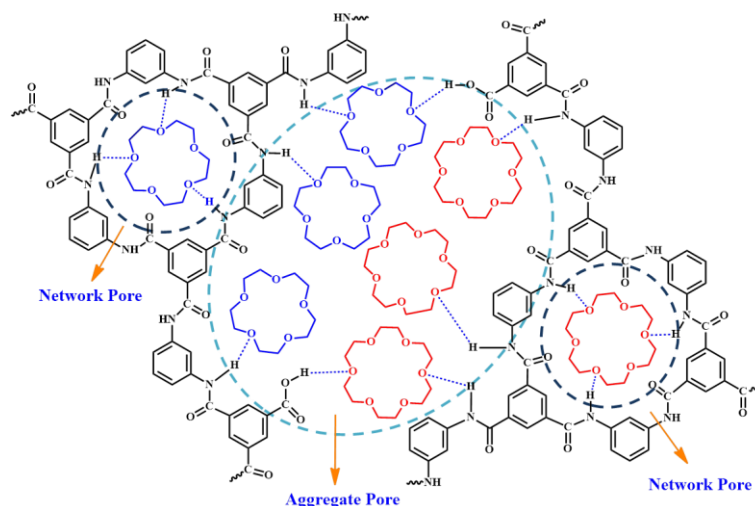
45 By 2050, the global population will increase by 2 billion, reaching 9.7 billion people.¹
46 Key to sustaining this burgeoning growth is overcoming water scarcity for
47 anthropogenic activities.² Various water treatment technologies have been exploited in
48 the past few decades to produce clean water.³⁻⁶ For example, membrane-based
49 separation techniques such as ultrafiltration,^{7,8} nanofiltration,⁹⁻¹¹ reverse osmosis^{12,13}
50 and forward osmosis (FO)¹⁴⁻¹⁶ have been implemented at various levels for
51 desalination, wastewater and water treatment. The heart of the successful
52 implementation of these technologies is a high-performance membrane with superior
53 separation efficiency and excellent fouling resistance. Since the commercialization of
54 thin-film composite (TFC) membranes in the 1970s,¹⁷ such membranes are preferred
55 in the industry for their high fluxes, reasonable selectivity and ease of fabrication.
56 TFC membranes are generally produced by interfacial polymerization (IP) of aromatic
57 amine monomers dissolved in an aqueous solution and an organic solution containing
58 acyl chloride monomers to form a dense aromatic polyamide (PA) layer on a porous
59 support layer.¹⁸⁻²¹ Both the reaction rate and degree of the polymerization are
60 determined by the solubility of the reactive monomer in the opposite phases i.e. the
61 diffusion rate of amine monomers from the aqueous phase into the organic phase.²²
62 Hence the diffusion-limited growth of PA chains coupled with the extremely fast
63 polymerization kinetics between both highly reactive monomers typically result in
64 poor control over bulk properties and microstructure of the formed PA layer,
65 consequently impacting on the separation performances of resulting TFC membranes.

66 The IP process can be tailored *via* various approaches to enhance separation
67 properties from an optimized PA microstructure. For example, the addition of catalytic

68 additives²³ in the monomer solution or a co-solvent system²² altered diffusion rates of
69 amine monomers into the organic phase and IP kinetics that consequently optimized
70 bulk properties and enhanced separation performances. Alternatively, effervescence
71 i.e. formation of nanosized gas bubbles in the amine solution *via* ultrasonication or
72 addition of NaHCO₃ to the amine solution also impacted on the morphology and
73 separation performances of TFC membranes.²⁴ Similarly, we recently showed that
74 ultrasonication during IP was effective for facilitating efficient mixing of two
75 monomer phases that optimized free volume size and content in the PA layer.^{25,26}
76 Additionally, the thickness, roughness and chemical composition of the PA layer
77 could be controlled by molecular layer-by-layer deposition method reported recently,
78 to yield maximum separation performances, where molecular transport was not
79 impeded by kinetic and mass transfer limitations associated with the traditional IP
80 process.²⁷ It also can be achieved by employing an intermediate layer of nanostrands
81 that regulated the release of amine monomers at the water-hexane interface, providing
82 precise control over the PA morphology and thickness.²⁸ Besides, 3D printed PA
83 membranes developed by electrospraying of monomers on to a substrate also
84 provided precise control over film thickness and roughness.²⁹ Recently, Wang *et. al.*
85 reported a nanostructure-mediated IP process to prepare rough PA layers with
86 extensively crumpled nanoscale structures.³⁰ The combination of these unique
87 nanoscale membrane topologies led to unprecedented permeances, which were
88 realized by preloading sacrificial templating nanoparticles on a substrate.³⁰

89 Different from these studies, here we incorporated crown ethers (CE) in the
90 monomer solution to tailor the formation of aggregate and network pores within PA
91 selective layers of TFC membranes that were crucial for addressing the tradeoff
92 relationship between permeability and selectivity (**Figure 1**). These membranes were

93 applied in FO for the first time. CE, a cyclic polyether, is miscible with both water
94 and organic solvents³¹ and is an excellent chelating agent with intrinsic cavities that
95 are selective towards metal ions (especially for alkali metal ions).³² Therefore, it is
96 widely used as the phase-transfer catalyst in organic reactions to transfer inorganic
97 reaction reagents into the organic phase, accelerating chemical reactions.³² Moreover,
98 the inner and outer of the CE cavity are hydrophilic and lipophilic, respectively.
99 Ascribing to these unique characteristics of CE, we hypothesized that CE-assisted IP
100 could significantly impact on the microstructure, morphology as well as FO
101 performances of resulting TFC membranes. This hypothesis was underpinned by two
102 main attributes. First, the miscibility of CE with organic solvents such as hexane and
103 the ability to form hydrogen bonds with amine monomers enable CE to act as a
104 co-solvent and phase-transfer catalyst to enhance amine diffusion into the organic
105 phase, contributing to a more complete IP reaction. Second, the hydrophilicity of CEs
106 could be harnessed to improve the water permeance of resultant PA films during FO
107 whilst chelating metal ions of draw solutes (NaCl and KCl used in this study),
108 contributing to less draw solute leakage. We systemically verified these hypotheses
109 using a series of complementary characterization techniques to elucidate the effects of
110 various modification routes (adding in the aqueous or organic phase), CE type and
111 concentration, as well as the draw solute type are investigated systematically in this
112 study.



113

114 **FIGURE 1** Schematic illustration of PA networks with CE15 and CE18 incorporated

115

116 2. EXPERIMENTAL

117

118 2.1 Materials

119

120 M-phenylenediamine (MPD, 99.5%) and 1, 3, 5-benzenetricarbonyl trichloride (TMC,
 121 98%) were bought from Aladdin and kept in a refrigerator before use. Polysulfone
 122 (PSf) (Mw = 800,000 Da) was obtained from Beijing HWRK Chem co. Ltd. (China).
 123 PSf was dried overnight in a vacuum oven at 80 °C prior use. Polyethylene glycol 400
 124 (PEG 400, CP), N-methyl pyrrolidone (NMP, anhydrous, $\geq 99.5\%$), n-hexane ($\geq 97\%$,
 125 anhydrous), 18-crown-6 (CE18, 99%, powder), 15-crown-5 (CE15, 99%, liquid),
 126 sodium alginate (SA, Mw: 98.11), potassium dihydrogen phosphate (KH_2PO_4 , 99.5%),
 127 magnesium sulfate (MgSO_4 , 99%), sodium sulfate (Na_2SO_4 , 99%), sodium
 128 bicarbonate (NaHCO_3 , 99.5%), ammonium chloride (NH_4Cl , 99.5%), calcium
 129 chloride (CaCl_2 , 96%) and sodium chloride (NaCl , $\geq 99.5\%$) were purchased from
 130 China National Medicine Corporation.

131

132 2.2 Preparation of TFC membranes

133

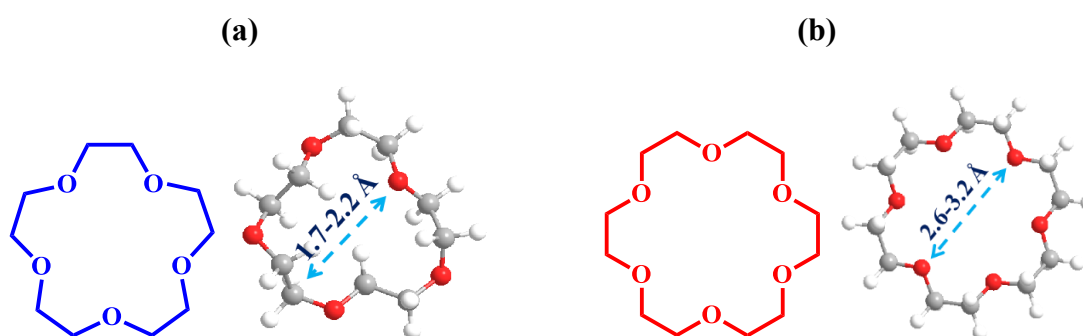
134 The PSf substrate membrane was fabricated using the non-solvent induced phase
135 separation method.^{33,34} Briefly, a degassed dope solution (PSf/PEG-400/NMP:
136 18/16/66 wt.%) was poured onto a clean glass plate and cast with a casting knife
137 (3520-8, Elcometer, UK) to obtain at thickness of 100 μm . The PSf substrate was
138 immediately immersed into a coagulation bath at room temperature to start the phase
139 inversion process. To remove trapped solvent molecules in the PSf substrate, the
140 water was changed every 12 hours for 2 days. These substrates were stored in
141 deionized (DI) water that was changed every 12 h to remove residual NMP.

142 CE-modified TFC membranes were fabricated by adding CE into the aqueous (1 –
143 9 wt.% of CE15 or 3 wt.% of CE18) or organic phase (3 wt.% of CE15 or CE18) prior
144 IP. Detailed compositions of the two monomer solutions studied here are listed in
145 **Table S1**. Depending on the type of CE used, 18-crown-6 or 15-crown-5,
146 CE-modified membranes were denoted as CE(A/O)-18/15-X where “A” and “O”
147 represents the deployment of CE in the aqueous or organic phase, respectively, and “X”
148 stands for the CE content. The miscibility of CE15 and solubility of CE18 in water
149 and hexane (**Figure S1** and **Table S2**) were exploited here to underpin in-situ
150 modification of PA selective layers of as-fabricated TFC membranes. The intrinsic
151 cavities of CE18 molecules ranged from 2.6 – 3.3 Å in diameter (**Figure 2**),^{32,35-37}
152 which are ideal for permeating water molecules (dynamic diameter of 2.6 Å).²²
153 Meanwhile, the cavity diameters of CE15 molecules are significantly smaller (1.7-2.2
154 Å) and are impermeable for water molecules.^{32,35-37} These differences in cavity
155 diameters also favor stable chelation of various cations where CE15 and CE18
156 molecules preferentially chelate Na^+ (1.90 Å) and K^+ (2.66 Å) ions, respectively.

157 ^{19,37,38} Pristine PSf membranes were immersed in an aqueous MPD/crown ether (3.4/0
158 – 9 wt.%) mixture for 2 min firstly. Excess MPD solution was removed carefully from
159 the substrate surface using a rubber roller. Next, the TMC/crown ether/hexane
160 solution (0.15/0 – 3/100 w/w/v) was poured on to the membrane top surface and left
161 for 1 min before draining off. The newly formed TFC membranes were washed with
162 DI water and stored in DI water before use.

163

164



166 **FIGURE 2** Molecular structures and intrinsic cavity diameter of (a) CE15 and (b)
167 CE18

168

169 **2.3 Characterizations of TFC membranes**

170

171 Changes in the chemical structures of TFC membranes were characterized using
172 Fourier Transform Infrared spectroscopy in the Attenuated Total Reflectance mode
173 (ATR-FTIR, Bruker, VERTEX-70) and X-ray Photoelectron Spectroscopy (XPS, VG
174 Multilab 2000, Thermo VG Scientific, UK) where a monochromatic Al K α X-ray
175 source was employed. The free volume content of the PA layer micro-structure was
176 characterized using Positron Annihilation Spectroscopy (PAS, National University of
177 Singapore) *via* a variable mono-energy slow positron beam.³⁹ The inter-chain distance
178 (*d*-spacing) of the PA layer was examined using X-ray diffractometer (XRD,

179 SmartLab-SE, Rigaku, Japan) with 2θ ranging from 10° to 60° . Surface hydrophilicity
180 of TFC membranes was evaluated using the water contact angle (WCA) measured by
181 a Contact Angle Goniometer (DSA 25, KRÜSS, Germany). Zeta potentials of TFC
182 membrane were measured at 25°C by a Zeta Potential Analyzer (SurPASS™ 3,
183 Anton Paar, Austria) using 0.001M KCl aqueous solution with pH of 2–10. The
184 surface morphology and topology of TFC membranes were observed by a Scanning
185 Electron Microscope (SEM, VEGA3, TESCAN, Czech) and Atomic Force
186 Microscope (AFM, SPM9700, Shimadzu, Japan) respectively.

187

188 **2.4 Evaluation of separation performance**

189

190 A lab-scale FO apparatus was employed to perform FO tests around $22\pm 0.5^\circ\text{C}$, using
191 DI water and 2.0 M NaCl aqueous solution as the feed and draw solutions,
192 respectively. All membrane samples were tested for at least three times under both FO
193 mode (active layer facing feed solution, AL-FS orientation) and PRO mode (active
194 layer facing draw solution, AL-DS orientation). Each test was stabilized for 30
195 minutes before data collection. Weight changes in the draw solution side were
196 detected by a digital weight balance (FX3000-GD, AND, Japan). Additionally,
197 concentration changes in the feed solution were monitored using a conductivity meter
198 (FE30, Mettler Toledo, Switzerland). Water flux (J_v) and reverse salt flux (J_s) were
199 determined to evaluate FO performance of TFC membranes, as defined by **Eqs. (1)**
200 **and (2)**.

$$201 \quad J_v = \frac{\Delta V}{A_m \Delta t} \quad (1)$$

$$202 \quad J_s = \frac{\Delta(C_t V_t)}{A_m \Delta t} \quad (2)$$

203 where ΔV is the volume change in the draw solution side over a predetermined time

204 (Δt), A_m is the effective membrane area in FO test (3.87 cm²), C_t and V_t are the salt
205 concentration and volume of the feed solution, respectively.

206

207 **2.5 Dynamic fouling tests**

208

209 Following well-established protocols described in our previous works,^{36, 37} we
210 performed dynamic fouling tests in the FO mode at 22±0.5 °C using synthetic
211 wastewater and 2.0 M NaCl aqueous solution as the feed and draw solutions,
212 respectively. Fresh membrane samples were stabilized by using DI water as both feed
213 and draw solutions for 30 min. The initial FO flux was measured after reaching steady
214 state by replacing DI water with 2 M NaCl solution as the draw solution. Next, the
215 fouling process was conducted by replacing DI water in the feed solution with
216 synthetic wastewater for 18 h (The fouling process time is 18 h using synthetic
217 wastewater as the feed solution). The flow rate in above stages were maintained at 0.3
218 L/min. Fouled membranes were flushed with DI water as both feed and draw
219 solutions at a flow rate of 0.6 L/min for 30 min. Finally, the FO fluxes of cleaned
220 membrane were measured again.

221

222 **2.6 Evaluation of CE stability in modified PA layers**

223

224 CE stability in the modified PA layer was evaluated by a long-term FO test and
225 vigorous agitation. For the long-term (72 h) FO test, a large amount of draw solution
226 (4 L 2 M NaCl or KCl solution) and feed solution (4 L DI water) were employed to
227 mitigate dilution effects of draw solutions and the concentration effects of feed
228 solutions. The vigorous agitation treatment was conducted by immersing fresh

229 membrane samples (25 cm²) into a centrifuge tube with 50 mL ultrapure water, which
230 was fixed in an oscillator for 7 days, with daily water changes. The amount of CE
231 released in the ultrapure water after various treatment durations were characterized
232 using a Total Organic Carbon analyzer (TOC, Vario, Elementar, Germany).

233

234 **3. RESULTS AND DISCUSSION**

235

236 **3.1 Modification mechanism**

237

238 The impact of CEs on the physicochemical structure of PA was characterized by FTIR
239 analyses and validated by XPS (**Figure 3**). From the FTIR spectra of membranes
240 studied here (**Figure 3a**), we observed peaks centered at 1624 and 1548 cm⁻¹ that
241 were characteristic to CO-NH groups i.e. amide bonds.⁴⁰ The presence of CE in
242 modified PA selective layers was validated by additional peaks centered at 1085 and
243 986 cm⁻¹ that are correlated to the ether functional group^{41,42} that are unique to CE
244 across all membranes studied in this work. Interestingly, the intensity of the peak
245 centered at 3460 cm⁻¹ (stretching vibration of -OH) was reduced in CE-modified
246 membranes. We hypothesize that the more complete IP reactions were facilitated by
247 CE-assisted amine diffusion/dissolution in the organic phase that resulted in efficient
248 mixing of both reactive monomers. This contradicts the principles of IP where amine
249 molecules are typically insoluble in organic phases.^{18,22} This hypothesis was validated
250 from FTIR analyses where hydrogen bonding between amine molecules and hexane
251 in the presence of CE were observed (**Figure S2**).

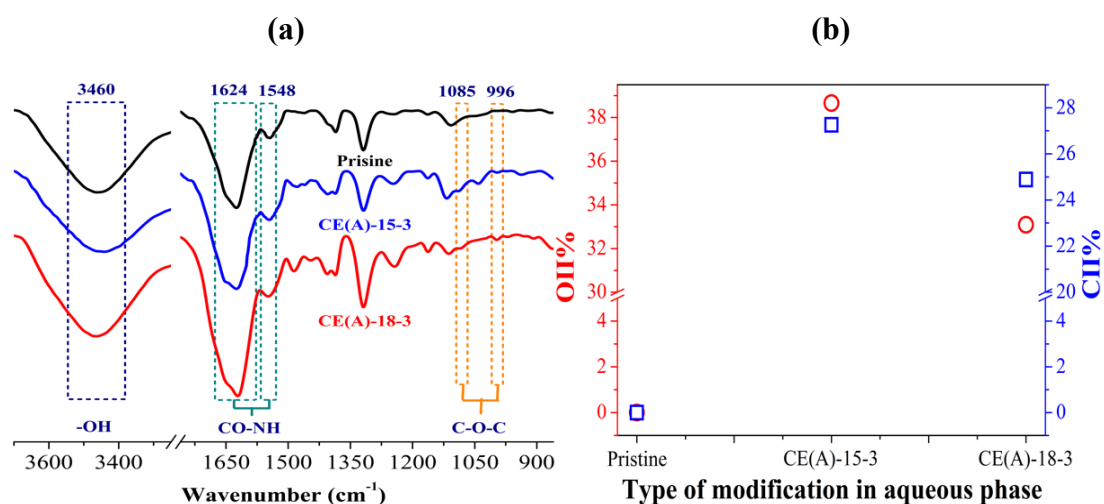
252 Quantitative evidence of CE presence in PA selective layers was observed from
253 XPS analyses (**Figure 3b**). OII (*O-C/H-*O-C/C-*O-C, BE=532.2 eV)⁴³ and CII

254 (*C-OR, BE=285.4 eV)⁴⁴ peaks that corresponded to ether functional groups were
255 only present in CE-modified PA membranes where both the OII% and CII% (peak
256 area ratio) of the CE15-modified membrane were larger than those modified by CE18
257 molecules (**Figure S3**). Based on our hypothesis, as more CE molecules are present,
258 the IP reaction would be more complete. This was also observed from the larger
259 increase in O/N ratio (**Table S3** and **Figure S4**) where N is unique to PA and the
260 increase in O content was primarily due to CE and higher intensity ratio of I_{OIII/OI}
261 (OIII corresponded to O atoms in carboxylic acid groups hydrolyzed from residual
262 TMC acyl chloride groups and OI was correlated to unreacted TMC carbonyl). Both
263 O/N and I_{OIII/OI} ratios of CE15-modified membranes were higher than those of
264 CE18-modified membranes. Attributing to a smaller molecular weight that facilitated
265 better diffusion of CE15 into hexane, the O/N ratio in PA membranes modified by
266 CE15 molecules was larger than that of membranes modified by CE18. TGA results
267 also revealed that weight losses of CE-modified PA powders in the second stage
268 (200-800 °C, caused by the thermochemical decomposition of PA chains) were lower
269 than those of pristine PA powders, possibly due to the intermolecular hydrogen bond
270 interaction between PA chains and embedded CEs, indicating the stable incorporation
271 of CEs in the PA network (**Figure S5**).

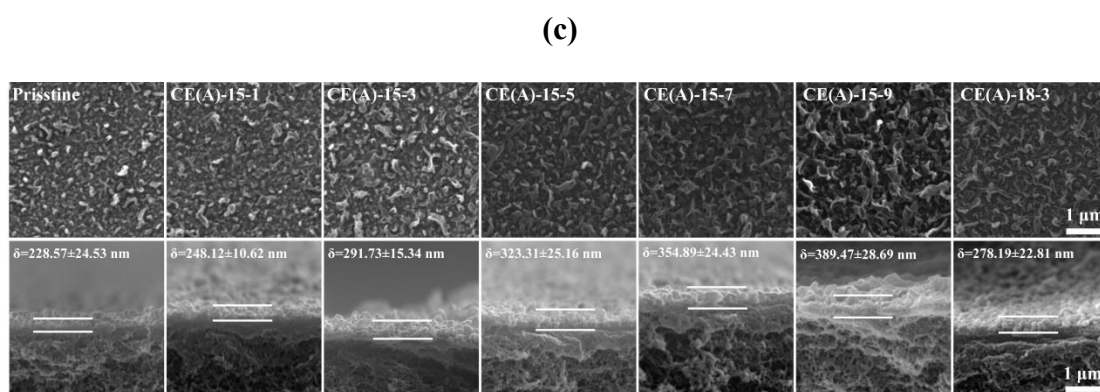
272 The deployment of CE as co-solvent or phase-transfer catalysts during IP also led
273 to the formation of rougher PA layers as confirmed by SEM and AFM images in
274 **Figures 3c-d**. **Figure 3c** also revealed that pristine PA membranes were thinner with
275 more nodular-like surfaces, while thicker CE-modified membranes comprised
276 obvious leaf-like and flake-like structures. Accordingly, as shown in **Figure 3d**, the
277 surfaces of CE-modified membranes were rougher than pristine membranes, and the
278 average roughness (*Ra*) increased with higher CE concentration or smaller CE

279 molecular weight (**Figure 3e**). However, the WCAs of CE-modified membranes were
 280 lower than those of pristine membranes, contradicting the *Ra* trends (**Figure 3e**). This
 281 was ascribed to the intrinsic hydrophilicity of CEs and rougher surface of
 282 CE-modified PA layers. Additionally, the lower carboxyl content in CE-modified PA
 283 i.e. higher IP conversion rates also attributed to higher zeta potential values at the
 284 same pH condition and the corresponding higher isoelectric points in CE-modified
 285 membranes (**Figure 3f**).

286
 287



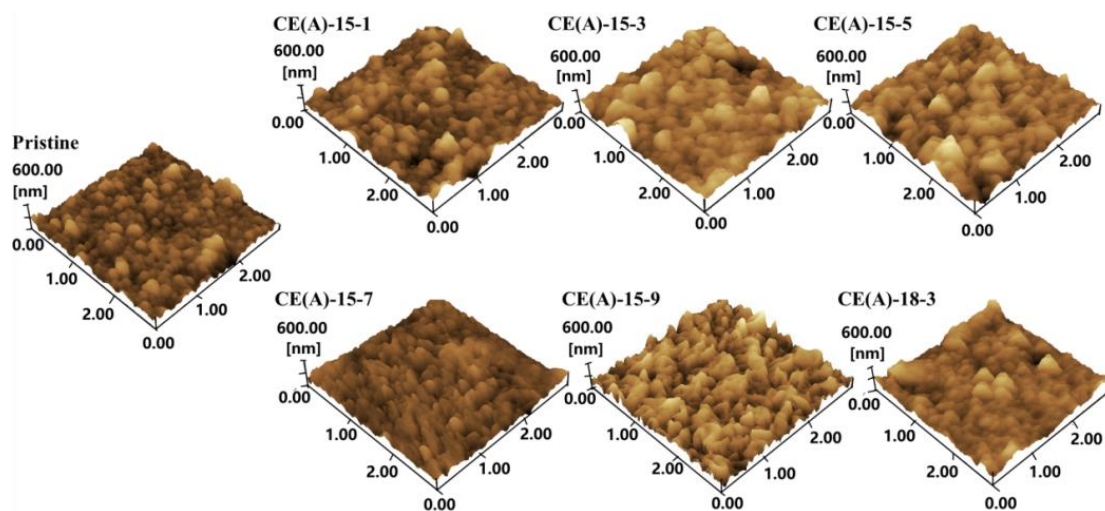
288
 289



290
 291

292

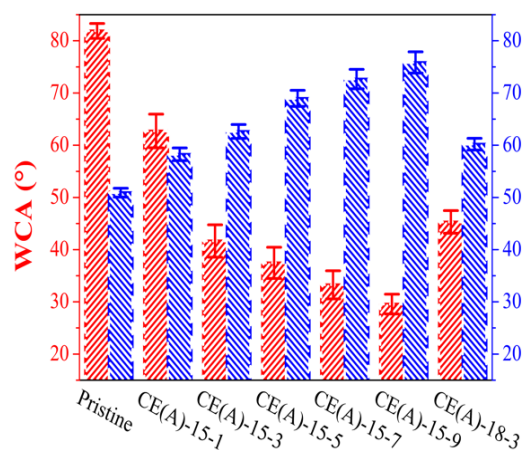
(d)



293

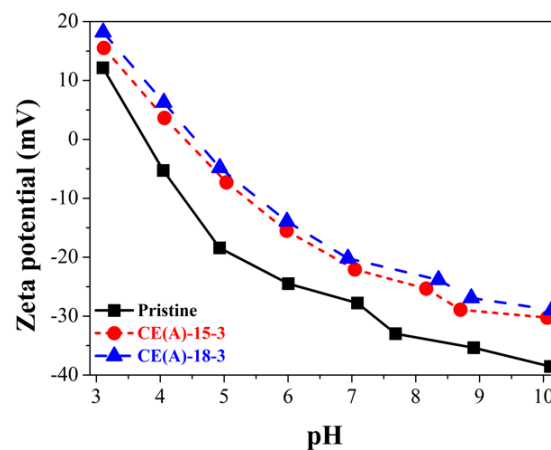
294

(e)



295

(f)



296 **FIGURE 3 (a)** FTIR spectra, **(b)** OII and CII peak area ratios, **(c)** SEM, **(d)** AFM, **(e)**
 297 water contact angles (WCA) and average roughness (Ra), **(f)** zeta potentials of the
 298 pristine and CE-modified membranes

299

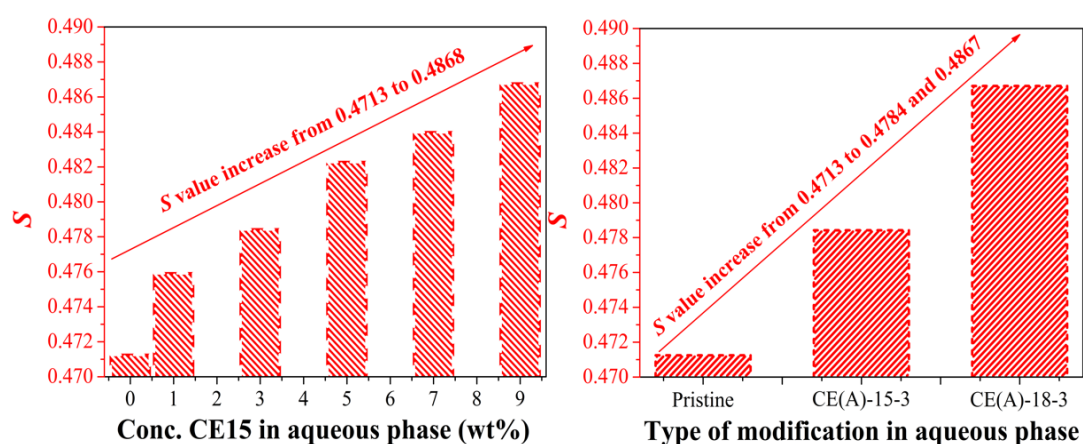
300 Structural changes induced by CE in the resulting PA layers were characterized by
 301 PAS and XRD (**Figure 4**). PAS results based on Doppler Broadening Energy
 302 Spectrum providing qualitative information about free volume, can be reflected by S
 303 parameter, which is defined as the ratio of total annihilation counts at central region
 304 (511 keV).^{45,46} Generally, S measures free volumes between 0.1 and 1 nm based on 2γ

305 annihilation. Higher S values typically indicate the more and/or larger free volume
 306 cavities in the polymer matrix, resulting in a looser structure.⁴⁵ In this study, S value at
 307 around 2 keV indicating the top PA layer was applied to estimate the free volume. S
 308 values in CE-modified membranes were larger than those of the pristine membranes
 309 (**Figures 4a** and **S6**), indicating the formation of looser PA layers with larger free
 310 volume content. The S value also increased as a function of CE15 content, CE
 311 molecular weight and intrinsic cavity size. Clearly, the effects of 9 wt.% of CE15 on
 312 microstructure and porosity could be achieved with 3 wt.% of CE18. The increases in
 313 free volume content and size were due to the enlargement of inter-PA chain distances
 314 caused by the addition of CE, where additives typically affect chain packing
 315 density.^{22,47} The interchain distance increased from 4.834 Å to 5.014 Å as CE15
 316 concentration increased from 1 to 9 wt.% (**Figures 4b** and **S7**). Meanwhile, the
 317 incorporation of 3 wt.% of CE18 could achieve the same effect as 9 wt.% of CE15,
 318 propping PA chains apart by 5.001 Å.

319

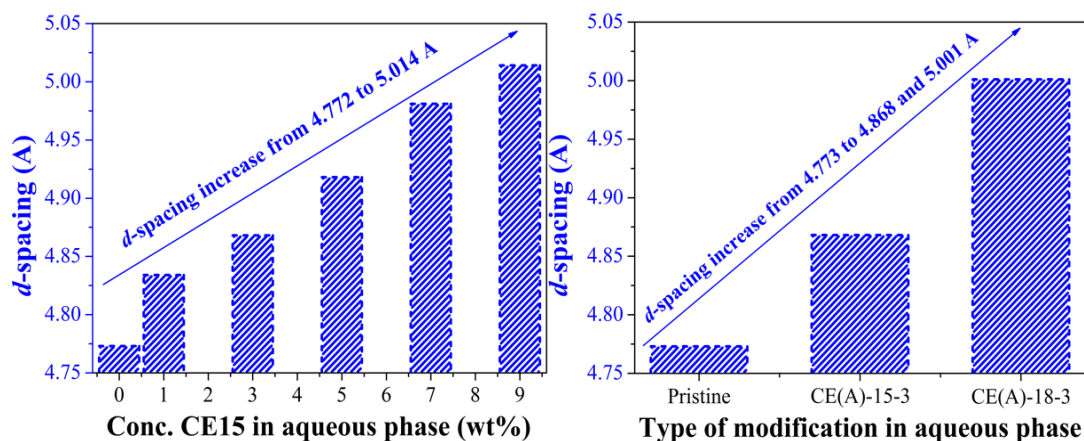
320

(a)



321

322



324

325 **FIGURE 4 (a) *S* and (b) *d*-spacing values of the pristine and CE-modified**326 **membranes**

327

328 **3.2 Separation performance, antifouling property, and long-term stability**

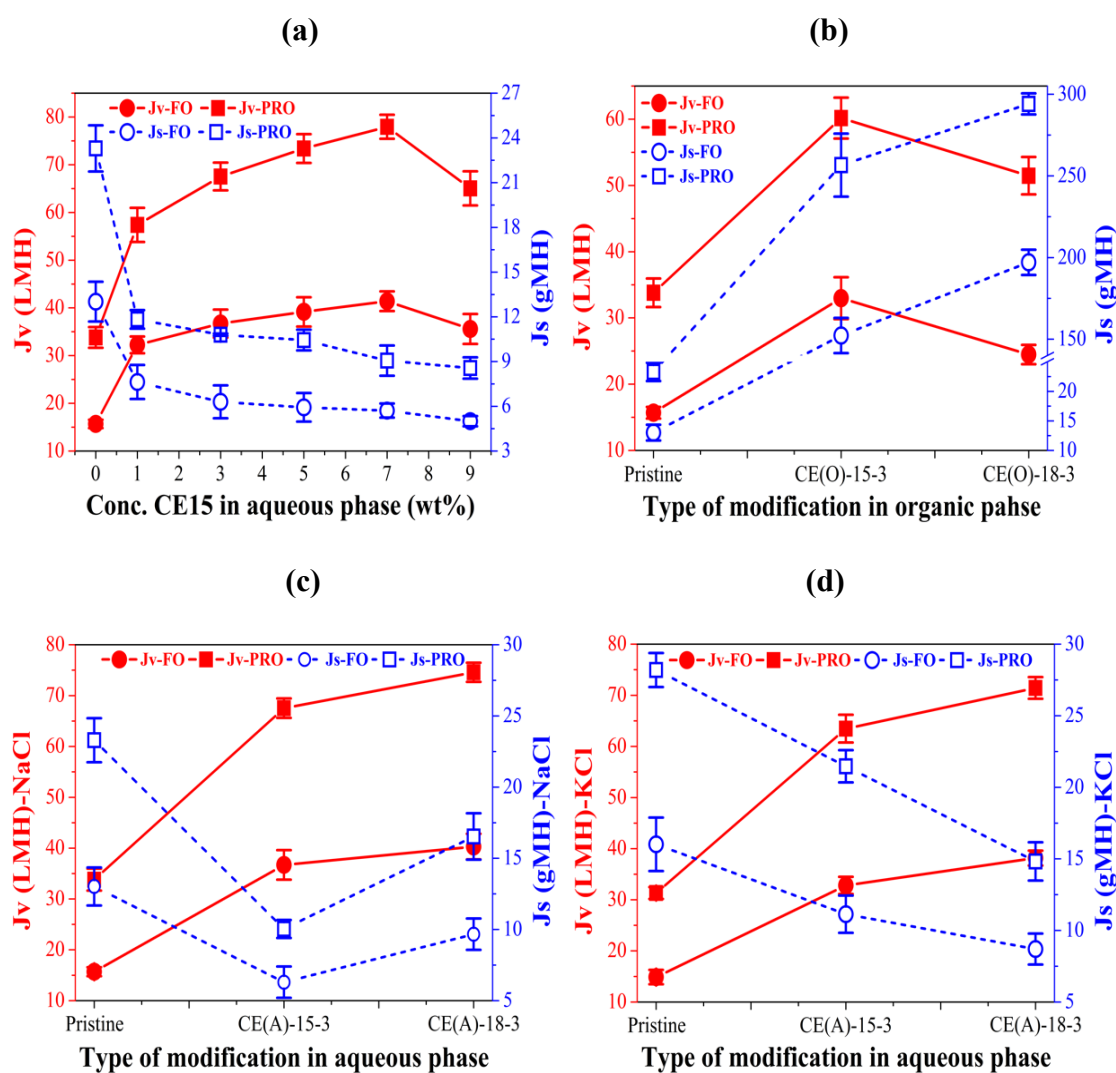
329

330 Compared to pristine PA membranes, the larger free volume, higher surface
 331 hydrophilicity and rougher surface (larger transport area for water molecules)⁴⁸ of the
 332 PA layers containing 1 – 7 wt.% CE15 enhanced water flux by 164% during FO
 333 operation were (**Figure 5**). However, as CE15 content increased to 9 wt.%, the
 334 thickness of the selective layer increased to 389.47 ± 28.69 nm that consequently
 335 reduced the water flux by 14% and 17% in FO and PRO modes respectively. Different
 336 from typical membrane modifications that increase reverse salt fluxes, the addition of
 337 CE15 reduced reverse salt fluxes as a function of higher CE content during
 338 modification. This was due to the combination of thicker PA layers, the chelation of
 339 CE15 with sodium ions and the repulsion effect of trapped NaCl molecules.

340 Alternatively, we added both CEs into the organic phase during IP. This approach
 341 was impractical as unstable membranes that discolored after IP were formed (**Figure**
 342 **S8**). Membrane discoloration observed here could be due to the dehydration of

343 amine-saturated substrates caused by CE attraction. Additionally, PA layers modified
 344 with CE in the organic phase became yellow and shrank after freeze drying, and
 345 delaminated from the discolored PSf substrate (**Figure S8**). PA delamination resulted
 346 from the inability to achieve polymer intrusion into the pores during IP, leading to less
 347 anchoring sites. The combination of delamination and poor chemical resistance in PA
 348 membranes modified with organic phase CE led to significantly higher water fluxes
 349 when compared to those of pristine membranes (**Figure 5b**). However, the reverse salt
 350 fluxes of these CE(O) membranes were also 11-15 times higher than that of pristine
 351 membranes.

352
 353



356
 357 **FIGURE 5** FO performance of the pristine membrane and modified membranes (**a**)

358 with different CE15 loadings added in the aqueous phase; **(b)** with different CEs
359 added in the organic phase; with different CEs added in the aqueous phase using **(c)**
360 NaCl or **(d)** KCl as the draw solution

361
362 To investigate the chelation ability of the CE15 and CE18 with Na⁺ and K⁺ ions,
363 respectively, we employed draw solutions that contained 2M NaCl or KCl draw
364 solution during FO separation (**Figures 5c-d**). The water fluxes of CE-modified TFC
365 membranes in both FO and PRO modes increased as a function of CE cavity size i.e.
366 water fluxes of CE-18 modified membranes were higher than that of CE-15 modified
367 membranes. The osmotic pressure of these two draw solutions were nearly equal,⁴⁹
368 hence resulting in 4-7% change in water flux, regardless membrane modification.
369 However, the reverse salt fluxes of these TFC membranes with the two different draw
370 solutions were vastly different. With NaCl draw solutions, the reverse salt flux of
371 pristine PA membranes was 23% and 21% lower than that with KCl draw solution
372 under FO and PRO mode. This was due to the smaller hydration radius of KCl. The
373 reverse salt flux of PA membranes modified with CE15 was reduced by 57%, from
374 23.29 gMH to 10.03 gMH when NaCl draw solutions were employed. The reduction
375 in reverse salt flux was only 24% CE15-modified PA membranes when KCl draw
376 solutions were employed. The lower reverse NaCl flux of CE15-modified membranes
377 was attributed to the stronger chelation ability between CE15 and Na⁺ ions, and
378 smaller hydration radius of KCl. However, this was not the case for CE18-modified
379 PA membranes where the reverse salt flux was lower when KCl draw solutions were
380 deployed during FO and PRO. This was in spite of the smaller hydration radius of

381 KCl when compared to NaCl molecules. Clearly, the chelation ability CE18 with K⁺
382 ions played a more dominant role here. Compare to CE15-modified membranes, the
383 reverse salt flux of CE18 membranes towards KCl draw solution was 31% lower,
384 even when the cavity size of CE18 molecules were larger. EDX characterization were
385 performed to quantify metal ion content in the membranes after FO tests (**Table 1** and
386 **Figure S9**). After FO test with NaCl draw solution, the Na content trapped in
387 CE15-modified membranes was 2.27%, 6 times higher than that in CE18-modified PA
388 membranes. Meanwhile, after FO test with KCl draw solution, K content in
389 CE18-modified membranes were 139% higher than that in CE15-modified
390 membranes, confirming the stronger chelation ability of CE18 with K⁺ ions.

391

392 **TABLE 1** Elemental composition of the pristine and CE-modified membranes after

393 FO tests using different draw solutes

Membrane code	C	N	O	Cl	Na	K
Pristine-NaCl	58.34	11.86	28.38	0.87	0.55	0.00
Pristine-KCl	58.61	10.18	30.16	0.63	0.00	0.42
CE(A)-15-3-NaCl	58.73	9.27	28.14	1.58	2.27	0.00
CE(A)-15-3-KCl	59.22	8.95	31.28	0.05	0.00	0.51
CE(A)-18-3-NaCl	58.75	9.50	31.36	0.09	0.30	0.00
CE(A)-18-3-KCl	58.35	6.53	32.74	1.17	0.00	1.22

394

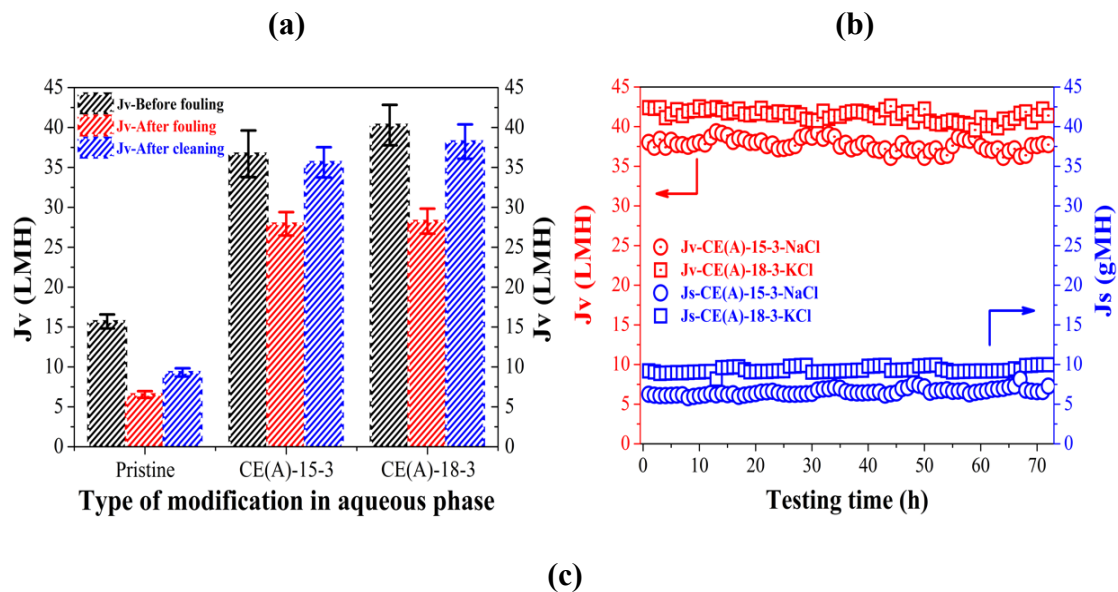
395 The fouling resistance of polymer membranes is crucial for determining the
396 quality of processed water and membrane lifespan.⁵⁰ Anti-fouling properties of

397 membranes studied here were investigated using synthetic wastewater containing SA
398 and calcium ions in the feed solution. Calcium ions acted as the bridge to crosslink SA
399 molecules, forming a SA gel layer on membrane surfaces.⁵¹ The formed SA gel layer
400 could enhance both transport resistance that reduces water permeation,⁵¹ and osmotic
401 pressure to significantly reduce the effective transmembrane osmotic pressure
402 difference.

403 Upon fouling, the water flux of pristine PA membranes was reduced by 60%,
404 reaching 6.5 LMH as shown in **Figures 6a** and **S10**. There as a 40% loss in water flux
405 even after physical cleaning as the water recovery ratio only reached 60%. Meanwhile,
406 the impact of fouling on the water flux of CE-modified membranes was less
407 prominent where water fluxes were reduced by 24% and 30% for CE15- and CE18-
408 modified membranes respectively. However, we were able to recover 95% of the
409 water flux after physical washes. The improved anti-fouling properties of
410 CE-modified membranes were ascribed to surface hydrophilicity and less reactive
411 carboxylic acid groups. The predominant factor was surface hydrohpilicity where the
412 oxygen atoms in CE behaved as hydrogen bond acceptors,⁵¹ attracting water
413 molecules onto the membrane surface to form a hydration layer that prevented the
414 adsorption of SA molecules. Additionally, the more complete IP reaction in
415 CE-modified membranes contained less carboxylic acid groups on the PA layer that
416 typically function as complexation sites to chelate calcium ions.^{51,52}

417

418



420

421

422

423

424

425

426

427

428

429

430

431

432

FIGURE 6 (a) Dynamic fouling test results of the pristine and CE-modified membranes; **(b)** long-term FO test results of CE-modified membranes; **(c)** FO performance comparison with recently reported TFC membranes with various modifications (DI water and 2 M NaCl used as the feed and draw solutions, PRO mode)

We also investigated the stability of embedded CE within the modified PA layers via long-term FO tests and vigorous shaking treatments. CE-modified membranes exhibited stable water fluxes over continuous 72 h FO tests (**Figures 6b** and **S11**). Additionally, the reverse salt fluxes of CE-modified membranes increased by only

433 9-12%, which was possibly due to the concentration effect of the feed solution. The
434 above results demonstrated that the FO performance of CE-modified TFC membranes
435 could be maintained in long term operation, inferring the stability of CE modifiers in
436 modified PA layers during FO operation. PAS and XRD characterization of
437 membranes after long term FO operation revealed that the S parameter value
438 decreased by 0.10-0.11% and the d -space decreased by 0.25-0.28% Å (**Table 2 and**
439 **Figure S12**). These slightly smaller values suggested that the decrease in the free
440 volume content of modified membranes was mainly underpinned by a reduction in
441 intrinsic cavity free volume of CEs. It also could indirectly reflect that the increment
442 in the free volume of CE-modified PA layer was mainly contributed by the larger
443 aggregate and network pores (i.e. the enlarged spatial distance)²². We also deployed a
444 TOC analyzer to characterize the amount of CE released from the membranes after
445 vigorous shaking (**Figure S13**). The average CE release rates of CE15-membranes
446 and CE18-membranes during the 7-day shaking treatment are 0.064 ± 0.02 and
447 0.055 ± 0.01 ppm/cm²·day, respectively, which further confirmed the stable CE-driven
448 modification of the PA selective layer. The stability of CE modifications, creation of
449 additional porosity whilst facilitating complete IP reactions underpinned the superior
450 separation performances of PA membranes containing 7 wt.% of CE15 molecules.
451 The FO performance of this membrane was more superior than those of various
452 state-of-the-art TFC-PA membranes as displayed in **Figure 6c**,^{23,33,53-60} highlighting
453 the feasibility of our approach.

454

455

456 **TABLE 2** *S* and 2 theta values of CE-modified membranes before and after long term
457 FO tests

Membrane code	<i>S</i>	<i>d</i>-spacing (Å)
CE(A)-15-3	0.4784	4.868
CE(A)-15-3-NaCl	0.4779	4.856
CE(A)-18-3	0.4867	5.001
CE(A)-18-3-KCl	0.4864	4.987

458

459 **4. CONCLUSIONS**

460

461 In the present study, we investigated the use of two identical CEs, CE15 and CE18, as
462 additives in the aqueous monomer phase to modify the PA selective layer of resultant
463 TFC membranes. Miscibility with hexane and the ability to hydrogen bond with MPD
464 molecules render CE as an efficient phase-transfer catalyst and co-solvent that
465 facilitated the diffusion of MPD molecules into the organic phase during IP.
466 Consequently, PA layers with higher crosslinking degrees and rougher surfaces were
467 achieved. Additionally, the incorporation of CE into the PA layer imbued higher
468 membrane surface hydrophilicity and higher free volume content. This was ascribed
469 to the polar ether groups and intrinsic cavities in CE as well as the enlarged spatial
470 distance of PA chains. Moreover, in comparison with pristine PA membranes, the
471 water fluxes of CE-modified membranes were enhanced by 164% and increased with
472 higher CE concentration or larger CE variants. Crucially, the use of CE during IP
473 lowered reverse salt fluxes of CE-modified membranes. We also demonstrated that
474 chelation abilities with Na⁺ or K⁺ ions could be harnessed to tailor higher solute
475 rejections of CE15- and CE18-modified membranes with suitable draw solutions.
476 CE-modified membranes were less prone to fouling because of their higher surface

477 hydrophilicity and lower carboxylic content in the PA layer. The stable embedment of
478 CE into the modified PA layer was also testified by long-term FO test. More
479 importantly, our approaches of CE modification and CE-assisted IP produced FO
480 membranes with state-of-the-art separation performances in a facile manner. This
481 modification approaches could be extended to produce polymer membranes for
482 nanofiltration and gas separations, potentially impacting other important separation
483 applications.

484

485 **ACKNOWLEDGMENTS**

486 We thank the financial support from National Key Technology Support Program (no.
487 2014BAD12B06), National Natural Science Foundation of China (no. 21306058), and
488 Natural Science Foundation of Hubei Scientific Committee (no. 2016CFA001). We
489 also appreciate Prof. Tai-Shung Chung in National University of Singapore for PAS
490 characterization. Special thanks are also given to the Analysis and Testing Center, the
491 Analysis and Testing Center of Chemistry and Chemical Engineering School, and the
492 State Key Laboratory of Materials Processing and Die & Mould Technology, in
493 Huazhong University of Science and Technology for their help with material
494 characterizations.

495

496 **REFERENCES**

- 497 **1.** Jones S, Anderson M. Global population set to hit 9.7 billion people by 2050
498 despite fall in fertility. *The Guardian*. 2015.
- 499 **2.** Elimelech M, Phillip WA. The future of seawater desalination: energy,
500 technology, and the environment. *Science*. 2011;333(6043):712-717.
- 501 **3.** Cheng XQ, Wang ZX, Zhang Y, Zhang Y, Ma J, Shao L. Bio-inspired loose

- 502 nanofiltration membranes with optimized separation performance for
503 antibiotics removals. *Journal of membrane science*. 2018;554:385-394.
- 504 **4.** Lieu Le N, Quilitzsch M, Cheng H, et al. Hollow fiber membrane lumen
505 modified by polyzwitterionic grafting. *Journal of Membrane Science*.
506 2017/01/15/ 2017;522:1-11.
- 507 **5.** Huang Y, Feng X. Polymer-enhanced ultrafiltration: Fundamentals,
508 applications and recent developments. *Journal of Membrane Science*. 2019.
- 509 **6.** Shen L, Zhang X, Zuo J, Wang Y. Performance enhancement of TFC FO
510 membranes with polyethyleneimine modification and post-treatment. *Journal*
511 *of Membrane Science*. 2017;534:46-58.
- 512 **7.** Le NL, Nunes SP. Ethylene glycol as bore fluid for hollow fiber membrane
513 preparation. *Journal of Membrane Science*. 2017/07/01/ 2017;533:171-178.
- 514 **8.** Le NL, Ulbricht M, Nunes SP. How do polyethylene glycol and poly
515 (sulfobetaine) hydrogel layers on ultrafiltration membranes minimize fouling
516 and stay stable in cleaning chemicals? *Industrial & Engineering Chemistry*
517 *Research*. 2017;56(23):6785-6795.
- 518 **9.** Huang Y, Sun J, Wu D, Feng X. Layer-by-layer self-assembled chitosan/PAA
519 nanofiltration membranes. *Separation and Purification Technology*.
520 2018;207:142-150.
- 521 **10.** Yao Z, Yang Z, Guo H, Ma X, Dong Y, Tang CY. Highly permeable and highly
522 selective ultrathin film composite polyamide membranes reinforced by
523 reactable polymer chains. *Journal of colloid and interface science*.
524 2019/09/15/ 2019;552:418-425.
- 525 **11.** Yi M, Lau CH, Xiong S, et al. Zwitterion-Ag Complexes That Simultaneously
526 Enhance Biofouling Resistance and Silver Binding Capability of Thin Film

- 527 Composite Membranes. *ACS applied materials & interfaces*. May 1
528 2019;11(17):15698-15708.
- 529 **12.** Yang Z, Guo H, Yao Z-k, Mei Y, Tang CY. Hydrophilic Silver Nanoparticles
530 Induce Selective Nanochannels in Thin Film Nanocomposite Polyamide
531 Membranes. *Environmental science & technology*. 2019;53(9):5301-5308.
- 532 **13.** Gai W, Zhao DL, Chung T-S. Thin film nanocomposite hollow fiber
533 membranes comprising Na⁺-functionalized carbon quantum dots for brackish
534 water desalination. *Water research*. 2019;154:54-61.
- 535 **14.** Shen L, Xiong S, Wang Y. Graphene oxide incorporated thin-film composite
536 membranes for forward osmosis applications. *Chemical Engineering Science*.
537 2016;143:194-205.
- 538 **15.** Zhang X, Xiong S, Liu C-X, et al. Confining migration of amine monomer
539 during interfacial polymerization for constructing thin-film composite forward
540 osmosis membrane with low fouling propensity. *Chemical Engineering
541 Science*. 2019;207:54-68.
- 542 **16.** Shen L, Zhang X, Tian L, et al. Constructing substrate of low structural
543 parameter by salt induction for high-performance TFC-FO membranes.
544 *Journal of Membrane Science*. 2020;600:117866.
- 545 **17.** Hoehn HH, Richter JW. Aromatic polyimide, polyester and polyamide
546 separation membranes: Google Patents; 1975.
- 547 **18.** Lau WJ, Ismail AF, Misdan N, Kassim MA. A recent progress in thin film
548 composite membrane: A review. *Desalination*. 2012;287:190-199.
- 549 **19.** Shen L, Wang Y. Efficient surface modification of thin-film composite
550 membranes with self-catalyzed tris(2-aminoethyl)amine for forward osmosis
551 separation. *Chemical Engineering Science*. 2018;178:82-92.

- 552 **20.** Cao X-L, Guo J-L, Cai J, et al. The encouraging improvement of polyamide
553 nanofiltration membrane by cucurbituril-based host-guest chemistry. *AIChE*
554 *Journal*.n/a(n/a).
- 555 **21.** Lu T-D, Chen B-Z, Wang J, et al. Electrospun nanofiber substrates that
556 enhance polar solvent separation from organic compounds in thin-film
557 composites. *Journal of Materials Chemistry A*. 2018;6(31):15047-15056.
- 558 **22.** Kim SH, Kwak S-Y, Suzuki T. Positron annihilation spectroscopic evidence to
559 demonstrate the flux-enhancement mechanism in morphology-controlled
560 thin-film-composite (TFC) membrane. *Environmental science & technology*.
561 2005;39(6):1764-1770.
- 562 **23.** Shen L, Zuo J, Wang Y. Tris(2-aminoethyl)amine in-situ modified thin-film
563 composite membranes for forward osmosis applications. *Journal of Membrane*
564 *Science*. 2017;537:186-201.
- 565 **24.** Ma X-H, Yao Z-K, Yang Z, et al. Nanofoaming of Polyamide Desalination
566 Membranes To Tune Permeability and Selectivity. *Environmental Science &*
567 *Technology Letters*. 2018;5(2):123-130.
- 568 **25.** Shen L, Hung W-s, Zuo J, Zhang X, Lai J-Y, Wang Y. High-performance
569 thin-film composite polyamide membranes developed with green
570 ultrasound-assisted interfacial polymerization. *Journal of Membrane Science*.
571 2019;570-571:112-119.
- 572 **26.** Shen L, Hung W-s, Zuo J, et al. Effect of ultrasonication parameters on
573 forward osmosis performance of thin film composite polyamide membranes
574 prepared with ultrasound-assisted interfacial polymerization. *Journal of*
575 *Membrane Science*. 2020;599:117834.
- 576 **27.** Gu JE, Lee S, Stafford CM, et al. Molecular layer-by-layer assembled

- 577 thin-film composite membranes for water desalination. *Advanced materials*.
578 Sep 14 2013;25(34):4778-4782.
- 579 **28.** Karan S, Jiang Z, Livingston AG. Sub-10 nm polyamide nanofilms with
580 ultrafast solvent transport for molecular separation. *Science*.
581 2015;348(6241):1347-1351.
- 582 **29.** Chowdhury MR, Steffes J, Huey BD, McCutcheon JR. 3D printed polyamide
583 membranes for desalination. *Science*. 2018;361(6403):682-686.
- 584 **30.** Wang Z, Wang Z, Lin S, et al. Nanoparticle-templated nanofiltration
585 membranes for ultrahigh performance desalination. *Nature communications*.
586 2018;9(1):2004.
- 587 **31.** Yoshio M, Noguchi H. Crown ethers for chemical analysis: A Review.
588 *Analytical Letters*. 1982;15(15):1197-1276.
- 589 **32.** Steed JW. First-and second-sphere coordination chemistry of alkali metal
590 crown ether complexes. *Coordination Chemistry Reviews*.
591 2001;215(1):171-221.
- 592 **33.** Shen L, Tian L, Zuo J, Zhang X, Sun S, Wang Y. Developing
593 high-performance thin-film composite forward osmosis membranes by various
594 tertiary amine catalysts for desalination. *Advanced Composites and Hybrid
595 Materials*. March 01 2019;2(1):51-69.
- 596 **34.** Shen L, Yi M, Tian L, et al. Efficient surface ionization and metallization of
597 TFC membranes with superior separation performance, antifouling and
598 anti-bacterial properties. *Journal of Membrane Science*. 2019;586:84-97.
- 599 **35.** Oehrle SA. Controlled changes in selectivity of cation separations by capillary
600 electrophoresis using various crown-ether additives. *Journal of
601 Chromatography A*. 1996;745(1-2):87-92.

- 602 **36.** Maleknia S, Brodbelt J. Cavity-size-dependent dissociation of crown
603 ether/ammonium ion complexes in the gas phase. *J.am.chem.soc.*
604 1993;115(7):2837-2843.
- 605 **37.** Ouchi M, Inoue Y, Kanzaki T, Hakushi T. Molecular design of crown ethers. 1.
606 Effects of methylene chain length: 15-to 17-crown-5 and 18-to 22-crown-6.
607 *The Journal of Organic Chemistry.* 1984;49(8):1408-1412.
- 608 **38.** Zhang H, Chu IH, Leming S, Dearden DV. Gas-phase molecular recognition:
609 gas-phase crown ether-alkali metal ion complexes and their reactions with
610 neutral crowns. *Journal of the American Chemical Society.*
611 1991;113(19):7415-7417.
- 612 **39.** Ong RC, Chung T-S. Fabrication and positron annihilation spectroscopy (PAS)
613 characterization of cellulose triacetate membranes for forward osmosis.
614 *Journal of membrane science.* 2012;394:230-240.
- 615 **40.** Belfer S, Purinson Y, Kedem O. Surface modification of commercial
616 polyamide reverse osmosis membranes by radical grafting: An ATR-FTIR
617 study. *Acta Polymerica.* 1998;49(10-11):574-582.
- 618 **41.** Gherrou A, Kerdjoudj H, Molinari R, Seta P, Drioli E. Fixed sites plasticized
619 cellulose triacetate membranes containing crown ethers for silver(I), copper(II)
620 and gold(III) ions transport. *Journal of Membrane Science.* 2004/01/15/
621 2004;228(2):149-157.
- 622 **42.** Li Y, Zhao JQ, Yuan YC, et al. Polyimide/Crown Ether Composite Films with
623 Necklace-Like Supramolecular Structure and Improved Mechanical, Dielectric,
624 and Hydrophobic Properties. *Macromolecules.* 2015/04/14
625 2015;48(7):2173-2183.
- 626 **43.** Kwon Y-N, Hong S, Choi H, Tak T. Surface modification of a polyamide

- 627 reverse osmosis membrane for chlorine resistance improvement. *Journal of*
628 *Membrane Science*. 2012/10/01/ 2012;415-416:192-198.
- 629 **44.** Chae H-R, Lee J, Lee C-H, Kim I-C, Park P-K. Graphene oxide-embedded
630 thin-film composite reverse osmosis membrane with high flux, anti-biofouling,
631 and chlorine resistance. *Journal of Membrane Science*. 2015;483:128-135.
- 632 **45.** Chen H, Hung W-S, Lo C-H, et al. Free-volume depth profile of polymeric
633 membranes studied by positron annihilation spectroscopy: layer structure from
634 interfacial polymerization. *Macromolecules*. 2007;40(21):7542-7557.
- 635 **46.** An Q, Hung W-S, Lo S-C, et al. Comparison between Free Volume
636 Characteristics of Composite Membranes Fabricated through Static and
637 Dynamic Interfacial Polymerization Processes. *Macromolecules*.
638 2012;45(8):3428-3435.
- 639 **47.** Kong X, Qiu Z-L, Lin C-E, et al. High permselectivity hyperbranched
640 polyester/polyamide ultrathin films with nanoscale heterogeneity. *Journal of*
641 *Materials Chemistry A*. 2017;5(17):7876-7884.
- 642 **48.** Tan Z, Chen S, Peng X, Zhang L, Gao C. Polyamide membranes with
643 nanoscale Turing structures for water purification. *Science*.
644 2018;360(6388):518-521.
- 645 **49.** Cath TY, Childress AE, Elimelech M. Forward osmosis: Principles,
646 applications, and recent developments. *Journal of Membrane Science*.
647 2006/09/15/ 2006;281(1):70-87.
- 648 **50.** Zhang R, Liu Y, He M, et al. Antifouling membranes for sustainable water
649 purification: strategies and mechanisms. *Chem Soc Rev*. Oct 24
650 2016;45(21):5888-5924.
- 651 **51.** Lu X, Romero-Vargas Castrillon S, Shaffer DL, Ma J, Elimelech M. In situ

- 652 surface chemical modification of thin-film composite forward osmosis
653 membranes for enhanced organic fouling resistance. *Environmental science &*
654 *technology*. 2013;47(21):12219-12228.
- 655 **52.** Xie M, Gray SR. Gypsum scaling in forward osmosis: Role of membrane
656 surface chemistry. *Journal of Membrane Science*. 2016;513:250-259.
- 657 **53.** Zhang X, Tian J, Ren Z, et al. High performance thin-film composite (TFC)
658 forward osmosis (FO) membrane fabricated on novel hydrophilic disulfonated
659 poly(arylene ether sulfone) multiblock copolymer/polysulfone substrate.
660 *Journal of Membrane Science*. 2016;520:529-539.
- 661 **54.** Qiu M, Wang J, He C. A stable and hydrophilic substrate for thin-film
662 composite forward osmosis membrane revealed by in-situ cross-linked
663 polymerization. *Desalination*. 2018;433:1-9.
- 664 **55.** Sukitpaneent P, Chung TS. High performance thin-film composite forward
665 osmosis hollow fiber membranes with macrovoid-free and highly porous
666 structure for sustainable water production. *Environmental science &*
667 *technology*. Jul 3 2012;46(13):7358-7365.
- 668 **56.** Widjojo N, Chung T-S, Weber M, Maletzko C, Warzelhan V. A sulfonated
669 polyphenylenesulfone (sPPSU) as the supporting substrate in thin film
670 composite (TFC) membranes with enhanced performance for forward osmosis
671 (FO). *Chemical Engineering Journal*. 2013;220:15-23.
- 672 **57.** Sahebi S, Phuntsho S, Woo YC, et al. Effect of sulphonated polyethersulfone
673 substrate for thin film composite forward osmosis membrane. *Desalination*.
674 2016;389:129-136.
- 675 **58.** Ghanbari M, Emadzadeh D, Lau WJ, Riazi H, Almasi D, Ismail AF.
676 Minimizing structural parameter of thin film composite forward osmosis

677 membranes using polysulfone/halloysite nanotubes as membrane substrates.
678 *Desalination*. 2016/01/01/ 2016;377:152-162.

679 **59.** Emadzadeh D, Lau WJ, Matsuura T, Ismail AF, Rahbari-Sisakht M. Synthesis
680 and characterization of thin film nanocomposite forward osmosis membrane
681 with hydrophilic nanocomposite support to reduce internal concentration
682 polarization. *Journal of Membrane Science*. 2014;449:74-85.

683 **60.** Shen L, Wang F, Tian L, Zhang X, Ding C, Wang Y. High-performance
684 thin-film composite membranes with surface functionalization by organic
685 phosphonic acids. *Journal of Membrane Science*. 2018;563:284-297.

686